Macromolecular Research, Vol. 16, No. 1, pp 6-14 (2008)

Rheology of PP/Clay Hybrid Produced by Supercritical CO_2 Assisted Extrusion

Sang Myung Lee, Dong Cheol Shim, and Jae Wook Lee*

Applied Rheology Center, Department of Chemical Engineering, Sogang University, Seoul 121-742, Korea

Received May 9, 2006; Revised September 17, 2007

Abstract: Polypropylene (PP)-layered silicate nanocomposites were developed using a new processing method involving a supercritical carbon dioxide ($scCO_2$)-assisted co-rotating twin-screw extrusion process. The nanocomposites were prepared through two step extrusion processes. In the first step, the PP/clay mixture was extruded with CO_2 injected into the barrel of the extruder and the resulting foamed extrudate was cooled and pelletized. In the second step, the foamed extrudate was extruded with venting to produce the final PP/clay nanocomposites without CO_2. In this study, organophilic-clay and polypropylene matrix were used. Maleic anhydride grafted polypropylene (PP-*g*-MA) was used as a compatibilizer. This study focused on the effect of $scCO_2$ on the dispersion characteristics of the clays into a PP matrix and the rheological properties of the layered silicate based PP nanocomposites. The dispersion properties of clays in the nanocomposites as well as the rheological properties of the nanocomposites were examined as a function of the PP-*g*-MA concentration. The degree of dispersion of the clays in the nanocomposites was analyzed by X-ray diffraction and transmission electron microscope. Various rheological properties of the nanocomposites were measured using a rotational rheometer. In the experimental results, the $scCO_2$ assisted continuous manufacturing extrusion system was used to successfully produce the organophilic-clay filled PP nanocomposites. It was found that $scCO_2$ had a measurable effect on the clay dispersion in the polymer matrix and the melt intercalation of a polymer into clay layers.

Keywords: nanocomposites, rheology, polypropylene, extrusion, supercritical fluid.

Introduction

Polymer layered silicate nanocomposites belong to a new class of hybrid materials of an organic polymer matrix in which silicates of nanoscale dimensions are imbedded. Two idealized nanocomposites are possible: intercalated and exfoliated. Intercalation results from the penetration of polymer chains into the interlayer region of the clay with preservation of the ordered layer structure. Exfoliation involves extensive polymer penetration and crystallite delamination, with the individual nanometer-thick silicate platelets are randomly dispersed in the polymer matrix. The silicates dispersed well in the polymer matrix improve dramatically thermal stability, mechanical properties, flame retardancy and gas permeability even with the small amount of silicates, compared to conventional composites. Many polymer systems have been investigated in this field, such as polyamide 6,[1-11] polystyrene,[12-20] poly(ethylene terephthalate),[21-22] polycarprolactone,[23-26] and epoxy resin,[27-32] etc.

Polypropylene (PP) is one of the most widely used thermoplastic materials in the polymer industry. PP/clay nanocomposite has viable applications in the industries of automobile, bottle, film, and package etc. However, because of non-polar characteristics of polypropylene, it is difficult to get the exfoliation and homogeneous dispersion of the silicate layer at the nanometer level in PP matrix. This is because the organophilic-clays have polar hydroxyl groups and are compatible only with polymers containing polar functional groups. Because of dispersion problem as above mentioned, many researchers, for the development of highly dispersed PP/clay nanocomposite, used PP-*g*-MA and hydroxyl groups grafted polypropylene (HOPP) containing polarity functional groups.[33-35] These coupling agents play a crucial role in dispersing the clay in the polymer matrix and in producing a strong interface between the two. However, in spite of their efforts, the development of the finely dispersed PP/clay nanocomposite at continuous process such as extrusion has been very difficult. In order to obtain homogeneous nanocomposite, not only material properties but also screw configuration, and operating condition must be considered as important variables.

In this study, to further enhance the nano-scale dispersion characteristics of clay in PP matrix, we introduced $scCO_2$ injection system to extrusion process for nanocomposite development.

$ScCO_2$ has characteristics such as gas-like diffusivity and

*Corresponding Author. E-mail: jwlee@sogang.ac.kr

viscosity, and liquid-like density. In particular, it has been used in a wide range of applications due to environmentally friendly and is lower critical point (31.1 °C, 73.8 bar), relatively low cost, nontoxic, and nonflammable compared to other supercritical fluids. With some exceptions, $scCO_2$ is a non-solvent for most polymers, however, it can plasticize most of them very efficiently. Due to its high compressibility, these solvent properties can be controlled by small changes in processing conditions, acting as a "reversible plasticizer" that can be easily removed after depressurization.[36]

The structure of nanocomposites is typically elucidated using X-ray diffraction (XRD) and transmission electron microscope (TEM). Whereas, TEM allows a qualitative understanding of the microstructure through direct visualization, wide-angle X-ray diffraction (WAXD) offers a convenient way to determine the interlayer spacing due to the periodic arrangement of silicate layers in the virgin clay and in intercalated nanocomposites. However, in the exfoliated or delaminated state where the periodic arrangement is lost, WAXD does not provide definitive information regarding the structure of the nanocomposite. WAXD can also suffer from problems of weak peak intensity, bias toward surface region, and poor resolution, particularly in those composites where the clay content is small.[37]

In this work, study on the development of enhanced continuous manufacturing process of PP/clay nanocomposite was carried out. Also, the effects of $scCO_2$ and PP-*g*-MA were investigated. Dispersion properties of clays in nanocomposites produced with and without $scCO_2$ were analyzed by WAXD. Rheological properties of nanocomposites at a microstructural level were also evaluated by rotational rheometer.

Experimental

Materials. The polymer used in this study was polypropylene (HP602N, Polymirae) whose density and MFR were 0.9 g/cm^3, and 12.5 g/10 min respectively. The average molecular weight, $\overline{M_w}$, was 222,400 and the polydispersity ratio, $\overline{M_w}$ / $\overline{M_n}$ = 5.23. Maleic anhydride modified polypropylene (PP-*g*-MA, grade Fusabond MD 353D, pellet type, produced from Dupont) with MA content of 3.2 wt% was used as the compatibilizer. The processing antioxidant (required to avoid oxidation during the process) was Irganox 8225 from Ciba specialty chemicals.

The organically modified montmorillonite (Closite 20A; it will be designated as C20A) was obtained from Southern Clay Products. C20A was the montmorillonite ion-exchanged with dimethyl dehydrogenated tallow ammonium ions.

Procedure. In order to develop homogeneous nanocomposite successfully, the metered CO_2 injection system assisted twin-screw extruder is introduced in this study as shown in Figure 1. The twin-screw extruder was a co-rotating, intermeshing twin screw extruder, SM Platek TEK25 with diameter 25 mm, total screw length of 1025 mm and a ratio of screw length to diameter (*L/D*) of 41. The metered

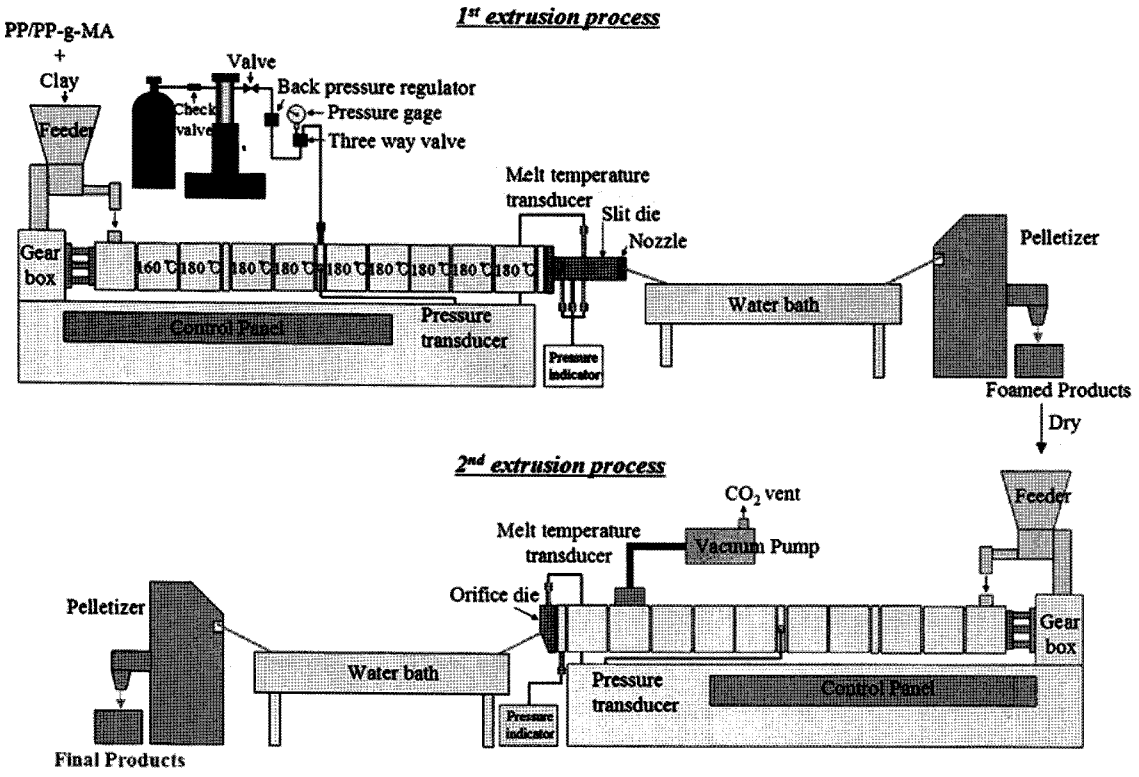

Figure 1. Manufacturing process of nanocomposite using $scCO_2$ assisted extrusion system.

Table I. Compositions of Polypropylene Nanocomposite

Sample	PP (part)	PP-*g*-MA (part)	C20A (part)
PPCN1	100	-	3
PPCN2	100	-	5
PPCN3	98	2	5
PPCN4	95	5	5
PPCN5	90	10	5
PPCN6	85	15	5
PPCN7	75	25	5

CO_2 injection system has a CO_2 cylinder, syringe pump, and back pressure regulator. Syringe pump (model 260D from ISCO, Inc.) was set to have CO_2 gas flow with a constant flow rate. Additionally, the back pressure regulator was used to maintain constant pressure. The processing of PP/clay nanocomposites was composed of two step extrusion processes (*see* Figure 1). The compositions of the hybrids are shown in Table I. In first step extrusion, CO_2 was injected into metering zone of extruder by CO_2 metered injection system and the foamed extrudate was pelletized after solidification in water bath. In order to build up the pressure over the critical pressure (73.8 bar) of CO_2, slit die and nozzle were used. In second step extrusion, CO_2 in the foamed product was vented by vacuum pump. The orifice die was equipped to depressurize die exit. Finally, the non-foamed PP/clay nanocomposites were obtained. The operating temperature profile for the extruder varied from 160 °C at the feed section to 180 °C at the die. The screw was arranged in a special combination of conveying, shearing, mixing, and reversing elements as shown in Figure 2. Reverse screw elements were inserted to elevate pressure profile in barrel and to increase residence time of melts. To confirm $scCO_2$ effect, the extrusion was also carried out without CO_2 injection (*see* Figure 2(b)).

Structural Characterization. Structural characterization (degree of delamination and dispersion) is carried out utilizing XRD and TEM.

The X-ray diffraction experiments were performed using Rigaku D/Max-A diffractometer (Cu Kα radiation with λ = 1.5406 Å) at room temperature. The 2θ angles were varying between 1.5 and 10° at a scanning rate of 1°/min in order to measure the d_{001}-spacing between silicate layers. The generator was operated at 40 kV and 40 mA.

Transmission electron microscope, Carl Zeiss LEO 912AB, was used to observe the dispersion of silicate in nanocomposites at an acceleration voltage of 160 kV. Nanometer sections are prepared from the pellets via melt compounded on the twin-screw extruder. Ultrathin sections of 100 nm in thickness, mounted on a 200 mesh copper grid, are cut using a microtome (Leica EM FCS) procedure with a diamond knife where the sample is held at room temperature to produce the uniform thin sections required to obtain clear reproducible images.

Rheological Characterization. The pellets are compression molded using a hydraulic press and 100 kg/cm^2 of pressure and 180 °C for 3 min. The compressed disks are 20 mm in diameter and 2 mm thick. Rheological properties of PP/clay nanocomposites produced at processing conditions with and without CO_2 were measured at 180 °C under the dynamic frequency sweep mode and relaxation test mode using a rotational rheometer (ARES from TA Inc.). In the

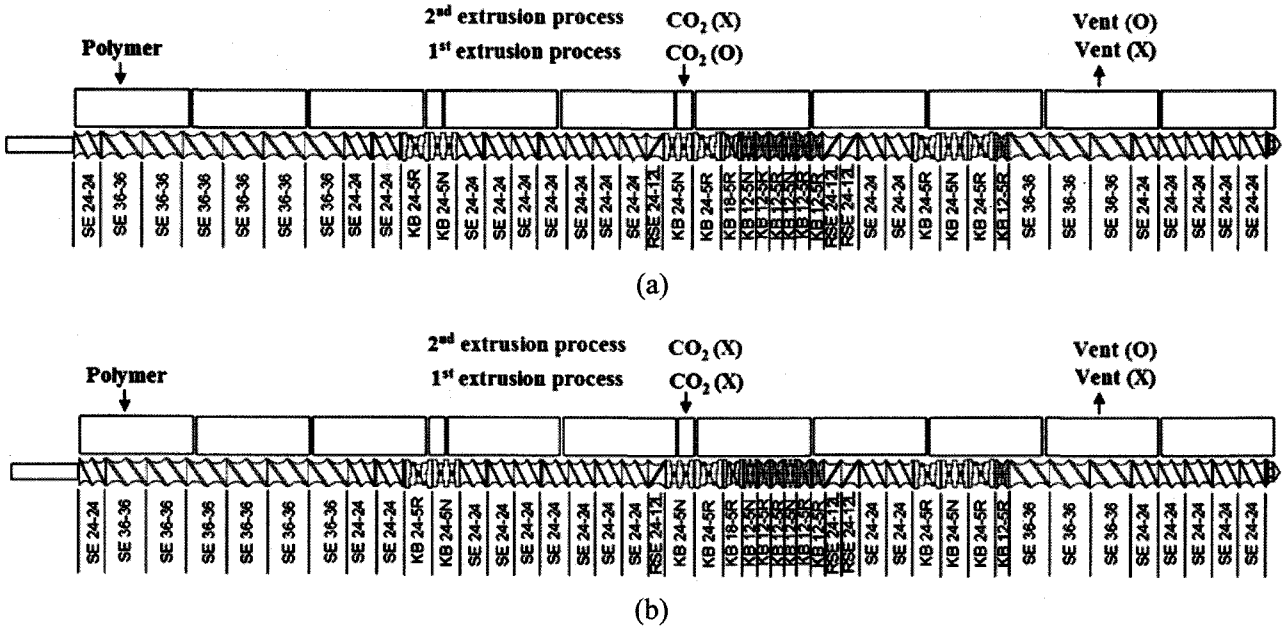

Figure 2. Screw configuration and processing conditions with and without $scCO_2$.

dynamic frequency sweep mode, a frequency range of 0.1~300 rad/s and strains of 10% are applied during the measurement. A strain sweep is preformed to verify that the strain amplitude is within the linear viscoelastic regime. The strain in relaxation test mode was 0.01%.

Results and Discussion

Effect of $scCO_2$ on Dispersibility of Clay. Polypropylene/clay nanocomposites are prepared both with and without the addition of CO_2. Figure 3 shows the XRD patterns of clay C20A, PPCN2, and PPCNs as a function of PP-*g*-MA concentration produced with the processing conditions without CO_2. PPCN2 is hybrid containing clay 5 wt%. The (001) plane peak of PPCN2 at processing condition without CO_2 was observed at $2\theta = 3.51°$ (25.2 Å), while the peak of the pure clay C20A was observed at $2\theta = 3.71°$ (23.8 Å). This indicates that little change has occurred in the basal spacing of the C20A in PPCN2. This is due to the incompatibility of the polar hydroxyl groups on the surface of the silicate layers and the non-polar PP.[38] However, the (001) plane peak of clay is reduced and is shifted to the lower angles in PPCNs as PP-*g*-MA concentration is increased. It is found that clays in PPCN6 and PPCN7 containing PP-*g*-MA of 15 and 25 wt% were practically exfoliated. Figure 4 shows XRD patterns of PPCN2 and PPCNs as a function of PP-*g*-MA concentration processed with CO_2 2 wt%. We confirmed that the addition of $scCO_2$ enhanced the chain diffusion and the clay dispersion as shown in Figure 4. Compared to the results of Figure 3, the (001) plane peaks of PPCN2 at the process with CO_2 2 wt% are shifted to the lower angles compared to PPCN2 processed without CO_2. The (001) plane peaks of PPCN2 at the process with CO_2 2 wt% was observed at $2\theta = 3.22°$, 27.4 Å. This clearly indicates an intercalation structure in PPCN2 processed

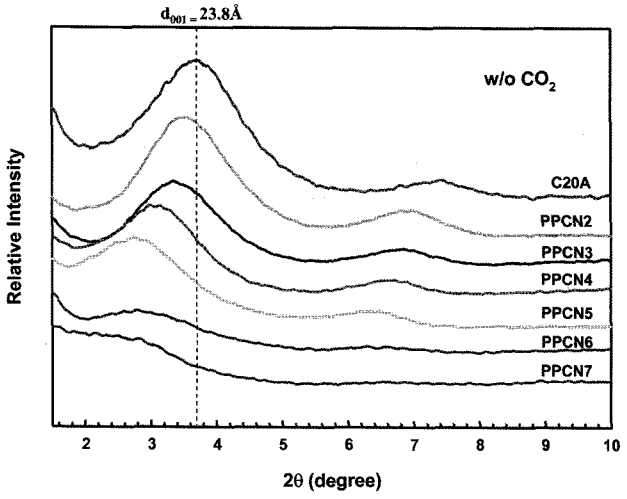

Figure 3. XRD patterns of PPCNs as a function of PP-*g*-MA concentration (w/o CO_2).

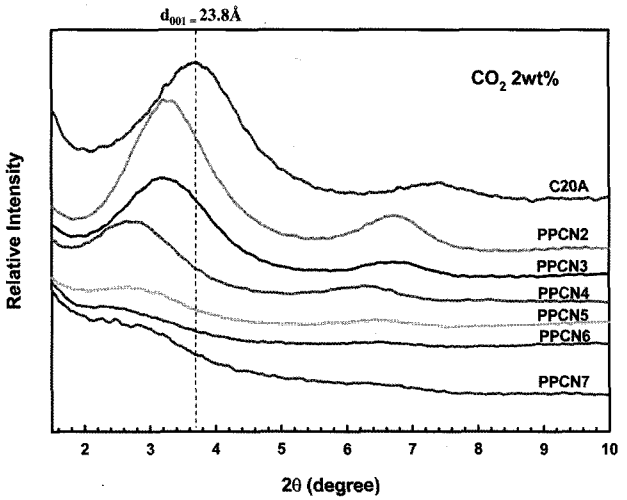

Figure 4. XRD patterns of PPCNs as a function of PP-*g*-MA concentration (CO_2 2 wt%).

with CO_2. This suggests a direct contribution of the presence of $scCO_2$ to the melt intercalation process, implying that in systems where diffusion of $scCO_2$ into silicate layers is present, the addition of $scCO_2$ can enhance the degree of intercalation. The possible mechanism for this result can be illustrated as following. $ScCO_2$ is diffused in silicate layers during the first step extrusion process. CO_2 leaves from silicate layers by its volume expansion and the reduction of pressure at die exit. Spaces between silicate layers that were occupied by CO_2 were replaced by PP chains. However, we confirmed that nanocomposites had intercalated state due to the incompatibility of the polar hydroxyl groups on the surface of the clay layers and the non-polar PP in spite of CO_2 introduced. The (001) plane peaks of clays in PPCN3 and PPCN4 containing PP-*g*-MA processed with CO_2 were shifted lower angles compared to that processed without CO_2. Additionally, PPCN5, which was produced without CO_2, shows the (001) plane peak of clay layers. In case of PPCN5 processed with CO_2 2 wt%, however, the (001) plane peak of clay layers is almost disappeared. Also, the level of dispersion of clays in PPCN6 and PPCN7 processed with CO_2 2 wt% was more improved compared to those processed without CO_2. Their properties are more clearly observed in TEM images. Figure 5(a) and (b) show TEM photomicrographs of PPCN3 and PPCN6 processed with and without CO_2 2 wt%. In TEM image of PPCN3 containing PP-*g*-MA 3 wt% processed without CO_2 (*See* Figure 5(a)), clay platelets were partially intercalated and exfoliated, but clay particle size is varied. On the other hands, particle size of clays in PPCN3 processed with CO_2 2 wt% is smaller compared to that in PPCN3 processed without CO_2. Also, dispersibility of clay particles is improved by the addition of $scCO_2$. In comparison with PPCN3 and PPCN6 as shown in Figure 5, it is confirmed that dispersibility of clays is improved and clays in PP matrix are more exfoliated as PP-*g*-MA concentra-

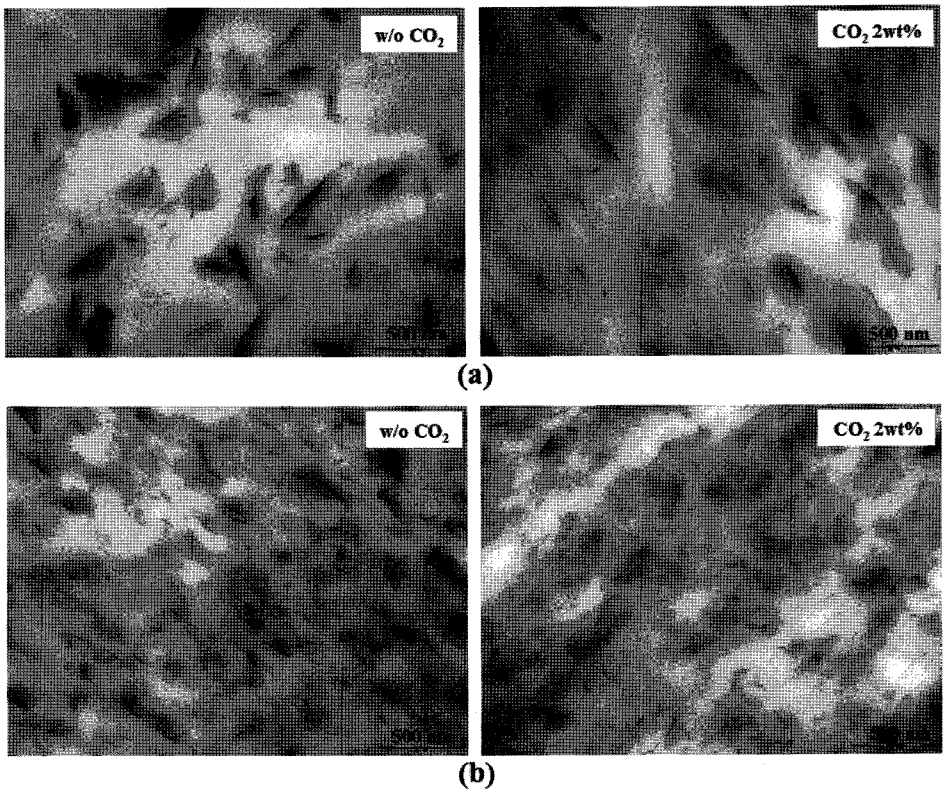

Figure 5. TEM images of PPCNs as a function of PP-*g*-MA concentration [(a) PPCN3 and (b) PPCN6].

tion is increased. As previous mentioned, it is found that the addition of $scCO_2$ increase dispersibility of clays in PP matrix. Besides the local analysis technique of XRD and TEM, the rheological characterization is also a sensitive method to reveal the global state of dispersion in the composites. In next section the rheological behavior of PPCNs will be discussed.

Rheological Properties of PPCNs. Understanding the rheological properties of nanocomposite melts is not only important in gaining a fundamental knowledge of the processibility, but is also helpful in understanding the structure-property relationships in these materials.[39] In this work, to understand the influence of various shear environments on nanocomposite system, the rheological behavior of nanocomposites have been studied.

Dynamic oscillatory shear measurements of polymeric materials are generally performed by applying a time dependent strain $\gamma(t) = \gamma_o \sin(\omega t)$, and measuring the resultant shear stress $\sigma(t) = \gamma_o [G' \sin(\omega t) + G'' \cos(\omega t)]$, where G' and G'' are the storage and loss moduli, respectively. In the case of polymer samples, it is expected at the frequencies at which the rheological measurements were carried should exhibit characteristic homopolymer-like terminal flow behavior, expressed by the power-laws $G' \propto \omega^2$ and $G'' \propto \omega$.

Figure 6(a) presents the complex viscosity PPCN1 as a function of CO_2. It can be seen that the complex viscosity of PPCN1 processed with CO_2 is higher compared to PPCN1 processed without CO_2. Especially, PPCN1 processed with CO_2 2 wt% shows the greatest enhancement in the complex viscosity. This is due to the degree of intercalation. The explanation for this will be introduced to Figure 8. Figure 6(b) shows the complex viscosity of PPCN2 as a function of CO_2. The rheological behavior of PPCN2 showed similar results with PPCN1 of Figure 6(a). The magnitude of complex viscosity of PPCN2 is generally higher than that of PPCN1 because clay concentration of PPCN2 is higher than that of PPCN1. However, the reason showing similar rheological pattern between neat PP and PPCN1/ PPCN2, is due to the incompatibility of the polar hydroxyl groups on the surface of the silicate layers and the non-polar PP. In Figure 7(a) and (b), storage moduli of PPCN1 and PPCN 2 as a function of CO_2 and clay concentrations, exhibited similar results to the behavior of the complex viscosity.

Figure 8 shows the (001) plane peaks of PPCN1 and PPCN2 as a function of CO_2 concentration. The (001) plane peaks of PPCN1 at processing conditions with CO_2 2 wt% has the lowest angle ($2\theta = 2.69°$, 32.8 Å). Also, the result of PPCN2 is similar to PPCN1. The (001) plane peaks of PPCN2 at processing conditions with CO_2 2 wt% has the lowest angle ($2\theta = 3.22°$, 27.4 Å). These results indicate existence of optimum concentration of CO_2.

Figure 9 shows complex viscosity versus angular fre-

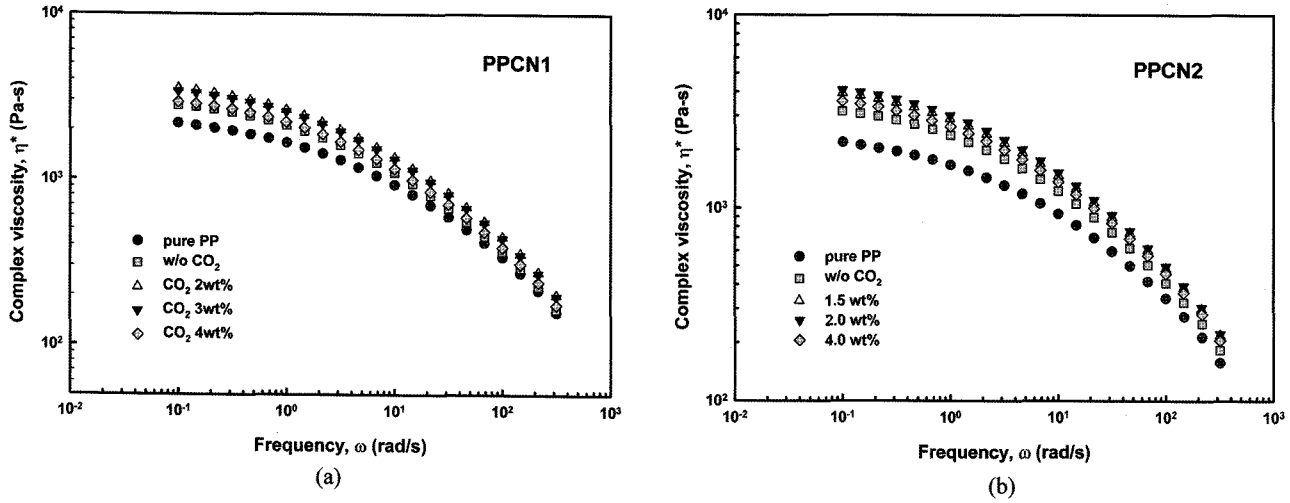

Figure 6. Rheological behaviors of PPCN1 and PPCN2 as a function of CO_2 concentration [(a) PPCN1 and (b) PPCN2].

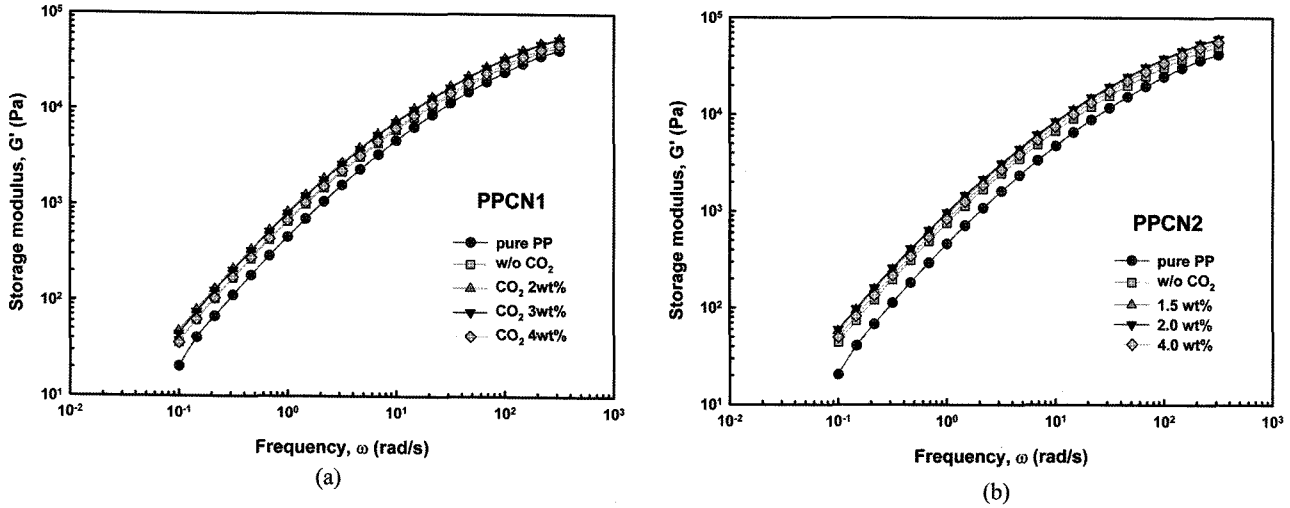

Figure 7. Rheological behaviors of PPCN1 and PPCN2 as a function of CO_2 concentration [(a) PPCN1 and (b) PPCN2].

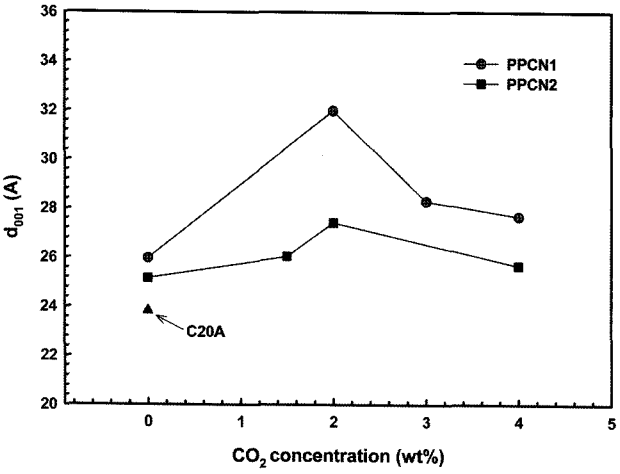

Figure 8. Gallery distances of clays in PPCNs.

quency at 180 °C for pure PP, PPCN2, and PPCNs as a function of PP-*g*-MA concentration processed without CO_2.

In case of PPCN2, its complex viscosity is larger than that for pure PP. However, PPCN2 shows Newtonian-like behavior similar to pure PP at low frequency range. This is due to the incompatibility of the polar hydroxyl groups on the surface of the silicate layers and the non-polar PP as discussed above. On the other hand, complex viscosity of PPCNs exhibits non-Newtonian behavior at low frequency range as PP-*g*-MA concentration increased. It clearly indicates that PP-*g*-MA can interact with layers of the clay through strong hydrogen bonding between the polar functional group of PP-*g*-MA and the polar hydroxyl groups on silicate clay layers. Non-Newtonian behavior like this is more clearly exhibited at PPCNs processed with CO_2 as shown in Figure 10. They reveal well dispersed structures, in agreement with the XRD and TEM results. The number of particles and dispersibility were increased with the addition of CO_2. This trend is more clearly observed in the plot of G' vs. ω, due to the extreme sensitivity of G' towards dispersed morphology

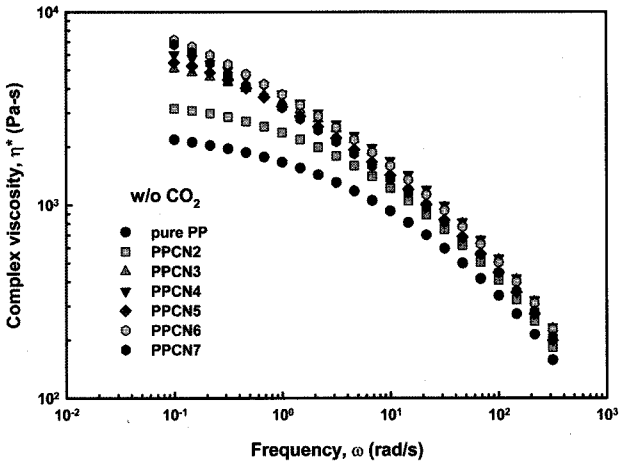

Figure 9. Complex viscosity of PPCNs as a function of PP-*g*-MA concentration (w/o CO_2).

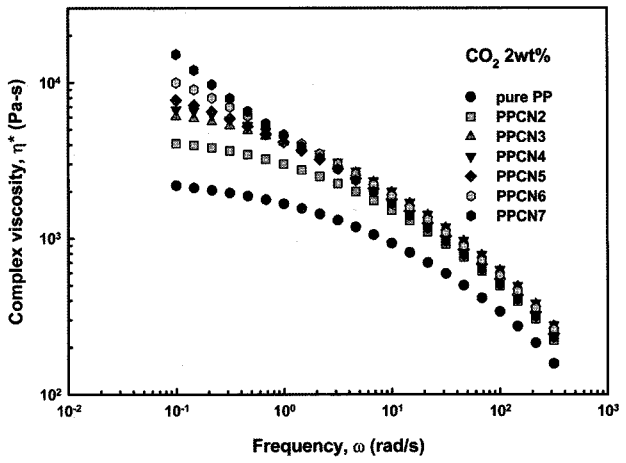

Figure 10. Complex viscosity of PPCNs as a function of PP-*g*-MA concentration (CO_2 2 wt%).

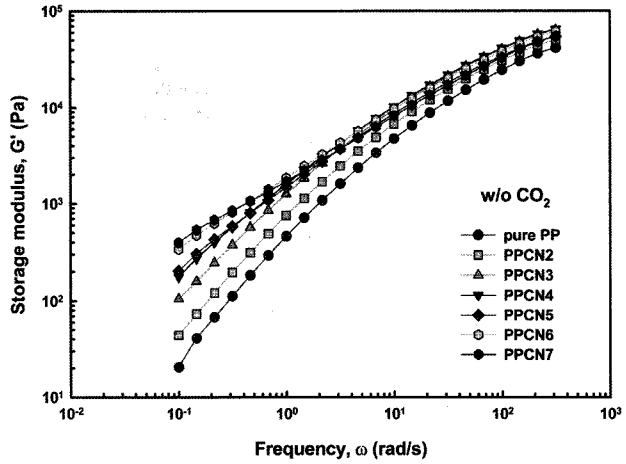

Figure 11. Storage modulus of PPCNs as a function of PP-*g*-MA concentration (w/o CO_2).

in the molten state. Figure 11 shows storage modulus versus angular frequency at 180 °C for pure PP, PPCN2, and

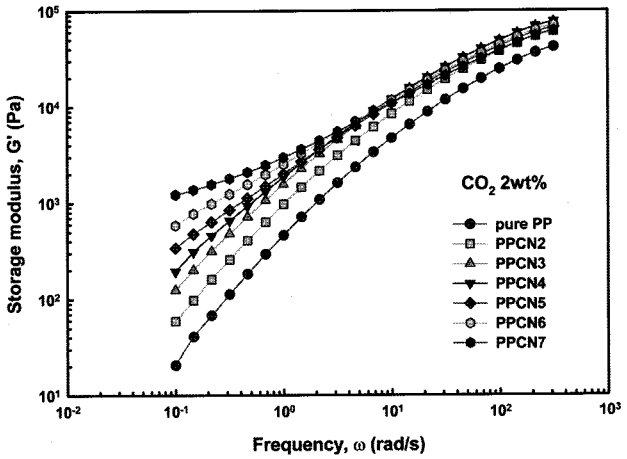

Figure 12. Storage modulus of PPCNs as a function of PP-*g*-MA concentration (CO_2 2 wt%).

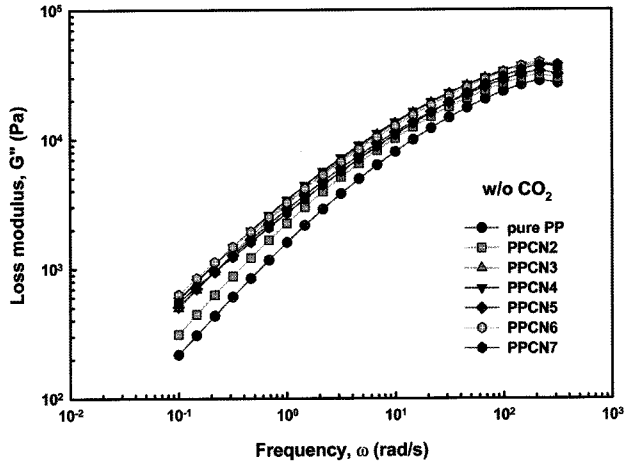

Figure 13. Loss modulus of PPCNs as a function of PP-*g*-MA concentration (w/o CO_2).

PPCNs as a function of PP-*g*-MA concentration at the processes without CO_2. The terminal zone slopes of PPCNs were decreased as PP-*g*-MA concentration increased, whereas the terminal slope for PPCN2 is approximately the same as pure PP. Such behavior at low frequency range is an indication of network formation involving the assembly of individual plates composed of silicate layers. This behavior corresponds to the shear thinning tendency, which appears strongly in the viscosity curves of PPCNs at low frequency ranges. PPCNs processed with CO_2 exhibit low terminal zone slope compared to PPCNs without CO_2 as shown in Figure 12. The terminal zone slopes of storage moduli for PPCNs processed with and without CO_2 are listed in Table II. The loss moduli of PPCNs processed without CO_2 showed similar behavior with their storage moduli as shown in Figure 13. PPCNs processed with CO_2 exhibit low terminal zone slope compared to PPCNs without CO_2 as shown in Figure 14. The terminal zone slopes of loss moduli for PPCNs processed with and without CO_2 are

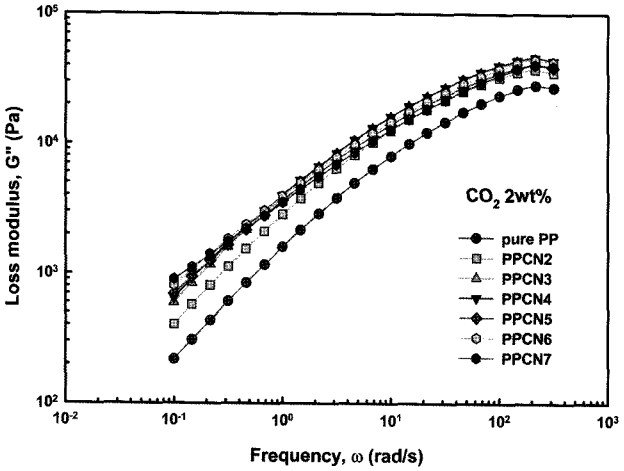

Figure 14. Loss modulus of PPCNs as a function of PP-*g*-MA concentration (CO_2 2 wt%).

Table II. The Terminal Zone Slopes of Storage Moduli for PPCNs Processed with and without CO_2

Sample	w/o CO_2	CO_2 2 wt%
	G' (Pa)	G' (Pa)
Pure PP	1.59	1.59
PPCN2	1.28	1.26
PPCN3	1.10	1.08
PPCN4	0.98	0.95
PPCN5	0.88	0.77
PPCN6	0.74	0.63
PPCN7	0.63	0.35

Table III. The Terminal Zone Slopes of Loss Moduli for PPCNs Processed with and without CO_2

Sample	w/o CO_2	CO_2 2wt%
	G'' (Pa)	G'' (Pa)
Pure PP	0.90	0.90
PPCN2	0.88	0.87
PPCN3	0.83	0.82
PPCN4	0.80	0.78
PPCN5	0.78	0.74
PPCN6	0.73	0.70
PPCN7	0.70	0.59

listed in Table III. The change of terminal zone slope for loss moduli of PPCNs as a function of PP-*g*-MA, however, is not severe compared to their storage moduli as shown in Tables II and III.

Conclusions

The $scCO_2$ assisted continuous manufacturing extrusion system was employed to successfully produce the organophilic-clay filled PP nanocomposites. It was found that $scCO_2$ had a measurable effect on the clay dispersion in polymer matrix and the melt intercalation of a polymer into clay nanoparticles in spite of the incompatibility of the polar hydroxyl groups on the surface of the silicate layers and the non-polar PP. This result is caused by the superior diffusion effect of $scCO_2$. Also, It was found that $scCO_2$ exert a favorable influence on the dispersion and exfoliations of clay in nanocomposites containing PP-*g*-MA. In view of the results of the rheological properties for PPCNs containing PP-*g*-MA, it is confirmed that clay intercalation or exfoliation within a PP matrix is accomplished by introducing pendant anhydride groups, which improve the strength of physical interactions at PP-clay interface.

Acknowledgments. The authors greatfully acknowledge the Korea Research Foundation Grant for the financial support (KRF-2006-005-J02302) and Brain Korea 21 Project.

References

(1) E. P. Giannelis, *Adv. Mater.*, **8**, 29 (1996).
(2) Y. Kojima, A. Usuki, M. Kawasumi, Y. Fukushima, A. Okada, T. Kurauchi, and O. Kamigaito, *J. Mater. Res.*, **8**, 1179 (1993).
(3) Y. Kojima, A. Usuki, M. Kawasumi, A. Okada, Y. Fukushima, T. Kurauchi, and O. Kamigaito, *J. Mater. Res.*, **8**, 1185 (1993).
(4) L. M. Liu, Z. N. Qi, and X. G. Zhu, *J. Appl. Polym. Sci.*, **71**, 1133 (1999).
(5) S. H. Wu, F. Y. Wang, C. M. Ma, W. C. Chang, C. T. Kuo, H. C. Kuan, and W. J. Chen, *Mater. Lett.*, **49**, 327 (2001).
(6) D. M. Lincoln, R. A. Vaia, Z. G. Wang, and B. S. Hsiao, *Polymer*, **42**, 1621 (2001).
(7) F. J. Medellin-Rodriguez, C. Burger, B. S. Hsiao, B. Chu, R. A. Vaia, and S. Phillips, *Polymer*, **42**, 9015 (2001).
(8) X. Liu and Q. Wu, *Polymer*, **43**, 1933 (2002).
(9) M. R. Kamal, N. K. Borse, and A. G. Rejon, *Polym. Eng. Sci.*, **42**, 1883 (2002).
(10) P. U. Arocha, C. Mehler, J. E. Puskas, and V. Altstadt, *Polymer*, **44**, 2441 (2003).
(11) J. H. Park, W. N. Kim, H. S. Kye, S. S. Lee, M. Park, J. K. Kim, and S. H. Lim, *Macromol. Res.*, **13**, 367 (2005).
(12) D. B. Zax, D. K. Yang, R. A. Santos, H. Hegmann, E. P. Giannelis, and E. Manias, *J. Chem. Phys.*, **112**, 2945 (2000).
(13) R. A. Vaia, H. Ishii, and E. P. Giannelis, *Chem. Mater.*, **5**, 1694 (1993).
(14) A. Alelah and M. Moet, *J. Mater. Sci.*, **31**, 3589 (1996).
(15) M. Sikka, L. N. Cerini, S. S. Ghosh, and K. I. Winey, *J. Polym. Sci.; Part B: Polym. Phys.*, **34**, 1443 (1996).
(16) M. Laus, M. Camerani, M. Lelli, K. Sparnacci, F. Sandrolini, and O. F. Francescangeli, *J. Mater. Sci.*, **33**, 2883 (1998).
(17) N. Hasegawa, H. Okamoto, M. Kawasumi, and A. Usuki, *J.*

Appl. Polym. Sci., **74**, 3359 (1999).
(18) M. W. Noh and D. C. Lee, *Polym. Bull.*, **42**, 619 (1999).
(19) X. Fu and S. Qutubuddin, *Polymer*, **42**, 807 (2001).
(20) F. L. Beyer, N. C. B. Tan, A. Dasgupta, and M. E. Galvin, *Chem. Mater.*, **14**, 2983 (2002).
(21) Y. C. Ke, C. Long, and Z. Qi, *J. Appl. Polym. Sci.*, **71**, 1139 (1999).
(22) C. H. Davis, L. J. Mathias, J. W. Gilman, D. A. Schiraldi, J. R. Shields, P. Trulove, T. E. Sutto, and H. C. Delong, *J. Polym. Sci.; Part B: Polym. Phys.*, **40**, 2661 (2002).
(23) P. B. Messersmith and E. P. Giannelis, *J. Polym. Sci.; Part A: Polym. Chem.*, **33**, 1047 (1995).
(24) G. Jimenez, N. Ogata, H. Kawai, and T. Ogihara, *J. Appl. Polym. Sci.*, **64**, 2211 (1997).
(25) R. Shima, L. A. Utracki, and A. Garcia-Rejon, *Compos. Interfaces*, **8**, 345 (2002).
(26) T. M. Wu, J. C. Cheng, and M. C. Yan, *Polymer*, **44**, 2553 (2003).
(27) P. B. Messersmith and E. P. Giannelis, *Chem. Mater.*, **6**, 1719 (1994).
(28) T. Lan, P. D. Kaviratna, and T. J. Pinnavaia, *Chem. Mater.*, **7**, 2144 (1995).
(29) C. Zilg, R. Mulhaupt, and J. Finter, *Macromol. Chem. Phys.*, **200**, 661 (1999).
(30) X. Kornmann, H. Lindberg, and L. A. Berhlund, *Polymer*, **42**, 1303 (2001).
(31) O. Becker, R. Varley, and G. Simon, *Polymer*, **43**, 4365 (2002).
(32) J. H. Park and C. H. Jana, *Polymer*, **44**, 2091 (2003).
(33) A. Usuki, M. Kato, A. Okata, and T. Kurauchi, *J. Appl. Polym. Sci.*, **63**, 137 (1997).
(34) H. R. Fischer and L. H. Gielgens, *Acta Polymerica*, **50**, 122 (1999).
(35) J. U. Park, J. L. Kim, D. H. Kim, K, H, Ahn, and S. J. Lee, *Macromol. Res.*, **14**, 318 (2006).
(36) J. F. Brennecke, *Nature*, **389**, 333 (1997).
(37) G. Galgali, C. Ramesh, and A. Lele, *Macromolecules*, **34**, 852 (2001).
(38) J. G. Ryu, J. W. Lee, and H. Kim, *Macromol. Res.*, **10**, 187 (2002).
(39) J. Y. Kim, S. H. Kim, S. W. Kang, J. H. Chang, and S. H. Ahn, *Macromol. Res.*, **14**, 146 (2006).